UC Davis
UC Davis Previously Published Works

Title

Reliability of arterial spin labeling derived cerebral blood flow in periventricular white matter

Permalink

https://escholarship.org/uc/item/4xc709f8

Journal

ISSN

Authors

Dolui, Sudipto
Fan, Audrey P
Zhao, Moss Y
et al.

Publication Date

DOI

Peer reviewed

Reliability of arterial spin labeling derived cerebral blood flow in periventricular white matter

Sudipto Dolui[a,*], **Audrey P. Fan**[b,c,d], **Moss Y. Zhao**[d], **Ilya M. Nasrallah**[a], **Greg Zaharchuk**[d], **John A. Detre**[a,e]

[a]Department of Radiology, University of Pennsylvania, PA, USA

[b]Department of Biomedical Engineering, University of California Davis, CA, USA

[c]Department of Neurology, University of California Davis, CA, USA

[d]Department of Radiology, Stanford University, CA, USA

[e]Department of Neurology, University of Pennsylvania, PA, USA

Abstract

We aimed to assess the reliability of cerebral blood flow (CBF) measured using arterial spin labeled (ASL) perfusion magnetic resonance imaging (MRI) from the periventricular white matter (PVWM) by computing its repeatability and comparing to [^{15}O]-water Positron Emission Tomography (PET) as a reference. Simultaneous PET/MRI perfusion data were acquired twice in the same session, about 15 min apart, from 16 subjects (age: 41.4 ± 12.0 years, 9 female). ASL protocols used pseudocontinuous labeling (pCASL) with background-suppressed 3-dimensional readouts, and included both single and multiple post labeling delay (PLD) acquisitions, each acquired twice, with the latter providing both CBF and arterial transit time (ATT) maps. The reliability of ASL derived PVWM CBF was evaluated using intra-session repeatability assessed by the within-subject coefficient of variation (wsCV) of the PVWM CBF values obtained from the two scans, correlation with concurrently-acquired PET CBF values, and by comparing them with that measured in other commonly used regions of interest (ROIs) such as whole brain (WB), gray matter (GM) and white matter (WM). The wsCVs for PVWM CBF with single and multi-PLD acquisitions were 5.7 (95% CI: (3.4,7.7)) % and 6.1 (95% CI: (3.8,8.3))%, which were similar to those obtained from WB, GM and WM CBF even though the PVWM region is the most weakly perfused region of brain parenchyma. Correlations between relative PVWM CBF derived from ASL and from [^{15}O]-water PET were also comparable to the other ROIs. Finally, the ATT of the PVWM region was found to be 1.27 ± 0.27s, which was not an outlier for the arterial circulation of the brain. These findings suggest that PVWM CBF can be reliably measured with the current state-of-the-art ASL methods.

*Corresponding author. Department of Radiology, University of Pennsylvania, 3710 Hamilton Walk, Goddard Labs, Office 321, Philadelphia, PA, 19104, USA. sudiptod@pennmedicine.upenn.edu (S. Dolui).

Keywords

1. Introduction

Cerebral small vessel disease (SVD) is among the most prevalent central nervous system disorders and has a key mechanistic role in both aging and dementia (Cannistraro et al., 2019; Cuadrado-Godia et al., 2018; Wardlaw et al., 2013). A major challenge in the investigation of cerebral SVD is that cerebral small vessel integrity cannot be visualized directly *in vivo* (Pantoni, 2010). Instead, white matter lesions (WMLs) detected as hyperintensities on Fluid Attenuated Inversion Recovery (FLAIR) T2 weighted structural brain MRI currently provide the most widely accepted biomarker of SVD (Prins et al., 2005), albeit reflecting downstream effects of SVD and potentially also non-vascular pathologies such as inflammation and neurodegeneration (Lee et al., 2016; Nasrallah et al., 2019).

Cerebral blood flow (CBF) provides a direct measure of microvascular functional integrity (Detre et al., 1998) and has been associated with WML volumes (Shi et al., 2016). Arterial spin labeled (ASL) perfusion MRI allows noninvasive quantification of CBF (Alsop et al., 2015; Detre et al., 1992), but most studies relating ASL CBF to SVD have considered large regions of interest (ROIs) encompassing gray matter (GM) or whole brain (WB) (Shi et al., 2016) to achieve sufficient signal-to-noise ratio from intrinsically noisy ASL MRI measurements. The ability of ASL to measure CBF in the white matter (WM) has been questioned because CBF in WM is much lower than in GM (van Gelderen et al., 2008). However, advances in ASL MRI acquisition strategies such as pseudocontinuous labeling and 3D readouts with background suppression of static brain signal (Alsop et al., 2015) now allow CBF to be measured reliably, including in white matter, particularly for ROI-based analysis (Zhang et al., 2016). Multiple studies have even measured CBF in penumbras of WMLs and showed that to predict future development of WMLs (Promjunyakul et al., 2015; Promjunyakul et al., 2018).

While all parenchyma is ultimately perfused by microvessels, CBF measured in cortex also reflects neurodegenerative changes based on the tight coupling between CBF and metabolism (Dolui et al., 2017, 2020) and ASL derived CBF maps can also potentially be contaminated by signal changes in large arteries (Alsop and Detre, 1996). In contrast, the periventricular white matter (PVWM) region is supplied exclusively by the terminal distributions of long arterioles less than 100 μm in diameter (Moody et al., 1990). Hence CBF measured in PVWM can potentially provide a purer measure of cerebral microvascular perfusion than WB or GM. Notably, PVWM is even more weakly perfused than WM as a whole (Dolui et al., 2019; Holland et al., 2008) and age-associated WMLs also appear first and most frequently in the PVWM region (Dolui et al., 2019; Habes et al., 2016), which is consistent with the notion that they primarily result from chronic progressive ischemia.

Accordingly, PVWM CBF may provide a predictive biomarker of cerebral SVD (Dolui et al., 2019).

We previously demonstrated that the PVWM region showed reduced CBF as compared to the rest of brain tissue and that the reduction was not attributable to partial volume effects with the ventricles or the presence of WMLs (Dolui et al., 2019). Here we sought to evaluate the reliability of ASL MRI methods for quantifying PVWM CBF at the single subject level. The recent advent of dual modality positron emission tomography (PET)-MRI systems has enabled cross-validation of MRI and PET CBF using concurrent measurements to minimize differences due to physiological variations in CBF (Werner et al., 2015; Zhang et al., 2014). [^{15}O]-water PET is considered the current gold standard method for measuring CBF (Xu et al., 2010), though the method requires exposure to ionizing radiation. An advantage of [^{15}O]-water PET compared to ASL MRI is that the decay rate for [^{15}O]-water PET is almost two orders of magnitude longer than that for blood or tissue T1, allowing much more tracer to accumulate even in weakly perfused regions. Furthermore, the method involves full dynamic acquisition of the tracer concentration allowing more accurate quantification of CBF and is more robust in subjects with varying arterial transit time. We leveraged the availability of previously acquired (Fan et al., 2017, 2019) [^{15}O]-water PET and state-of-the-art ASL MRI data obtained with background suppression, pseudocontinuous labeling, and both single and multiple post-labeling delays; the latter can provide a measure of arterial transit time (ATT) and a more accurate measure of CBF (Gunther et al., 2001; Wang et al., 2013). We aimed to assess the reliability of ASL derived PVWM CBF by computing its intra-session reproducibility, correlation with [^{15}O]-water PET measurements and comparing the results with WB, GM and WM.

2.   Materials and methods

2.1.   Cohort

Data from 16 middle aged healthy subjects (age: 41.4 ± 12.0, range = 22–62 years, 9 female) with no history of neurological disorders and no contraindications to MRI were considered for this study. The work has been carried out in accordance with the Code of Ethics of the World Medical Association, the study protocols were approved by the Stanford University Institutional Review Board and informed written consents were obtained from all the participants.

2.2.   PET/MRI acquisition and processing

The PET/MRI data were acquired at the Stanford University on a simultaneous time-of-flight (TOF)-enabled 3.0 T PET/MRI scanner (SIGNA; GE Healthcare, Waukesha, WI). Simultaneous acquisitions of PET and ASL-MRI scans were conducted twice about 15 min apart within the same session and without repositioning the subjects in between scans. For the PET perfusion data, each subject received an intravenous bolus injection of [^{15}O]-water (490–960 MBq). The first 2 min of PET counts after tracer administration were reconstructed to create a map of relative CBF. PET reconstruction was performed using a TOF- ordered subset expectation maximization (OSEM) algorithm on a 192 × 192 matrix,

30 cm field-of view, 2.78 mm slice thickness, and included correction for scatter, random counts, dead time, and point-spread function.

ASL MRI data were acquired using pseudo-continuous labeling, both with single and multiple PLD, and a 3-dimensional fast spin echo readout with stack-of-spirals readout trajectory. The single-PLD data were acquired with a labeling duration of 1.5s, PLD of 2.025s, TR/TE = 4852/10.7 ms, in-plane acquisition resolution of 3.7 mm and slice thickness of 4 mm and reconstructed to $1.9 \times 1.9 \times 4mm^3$, 8 spiral arms with 512 points/ arm, 3 averages. The multi-PLD data were acquired with a labeling duration of 2s and with 5 PLDs evenly spaced between 0.7 and 3s, TR/TE = 6489/10.7 ms, in plane acquisition resolution of 5.8 mm and slice thickness of 4 mm and reconstructed to $1.9 \times 1.9 \times 4mm^3$, 4 spiral arms with 512 points/arm, and single image for each PLD. High resolution 3-dimensional T1 -weighted scans were also obtained with an inversion-recovery prepared, fast spoiled gradient recalled sequence (TR = 9.5 ms; TE = 3.8 ms; spatial resolution = 0.93 $\times 0.93 \times 1$ mm^3).

The data were processed using standard processing pipelines (Fan et al., 2016; Fan et al., 2019) implemented in MATLAB and SPM12. Briefly, single-PLD ASL was processed and quantified using a single compartment model as recommended by Alsop et al. (2015). For multi-PLD ASL, the arterial transit time (ATT) maps were obtained using a weighted delay method described by Dai et al. (2012). Thereafter CBF was quantified using a 2-compartment model for each PLD, and the CBF maps for each delay time were combined through a weighted average to obtain the final CBF map (Dai et al., 2012; Fan et al., 2017). Note that the quantification models in single and multi-PLD ASL were different as they used single and two-compartment models respectively, but the goal of the study was to show the reliability of the ASL derived PVWM CBF values considering the assumptions associated with each modality. All the CBF maps were visually inspected for artifacts. The CBF maps were registered to the T1 image using normalized mutual information criteria in SPM12.

The T1 images were segmented into GM, WM and cerebrospinal fluid (CSF) tissue probability maps (TPMs) using SPM12 and whole brain ROIs for each subject were obtained by binarizing the sum of GM and WM tissue probabilities using a threshold of 0.85. Mean CBF in the whole brain was obtained for further analysis. To obtain mean GM and WM CBF for each subject, we performed partial volume correction of the CBF maps using the method of Asllani et al. (2008) where the anatomical priors of the method were derived from smoothing the GM and WM TPMs by the estimated effective resolutions of each modality. The effective resolution of single PLD values was estimated by Petr et al. (2018) to have a Gaussian full width at half max (FWHM) of $4.6 \times 4.3 \times 11.8$ mm^3. We used the same effective resolution (FWHM = 11.8 mm) in slice encoding direction for multi-PLD acquisition while using the effective in-plane resolution same as the nominal resolution (5.8 $\times 5.8$ mm^2). Finally, we used the PET effective resolution to have a FWHM of $4.5 \times 4.5 \times 4.5$ mm^3 as suggested by the physicists in the acquisition site and which matched closely with previous publications (Grant et al., 2016). Mean CBF in GM and WM were obtained from the PVC maps within regions having corresponding TPMs, corrected for effective resolution, greater than 0.6.

2.3. PVWM ROI definition from CARDIA data

In our previous work (Dolui et al., 2019), we constructed a functionally defined PVWM ROI based on the region of lowest perfusion in a sample of 436 subjects (age = 50.4 ± 3.5 years, 54% female) from the NHLBI Coronary Artery Risk Development in Young Adults (CARDIA) study (Dolui et al., 2016). The group averaged CBF map is shown in Fig. 1(A). The lowest CBF values, shown in blue, were found in the PVWM region, hence a PVWM ROI was constructed by including WM voxels with CBF values below an empirically set threshold of 12.5 ml/100 g/min, as illustrated in Fig. 1(B). Note that the CARDIA data were not used in any further analysis in thus study. The ROI was warped to the T1 space of each subject and PVWM CBF was extracted as the median of partial volume corrected WM CBF values within this ROI and having corrected WM tissue probabilities greater than 0.6. We used median to have a robust measure in the small PVWM ROI of relatively low CBF values.

2.4. Data analysis

2.4.1. Intra-session repeatability of ASL derived CBF—We evaluated the intra-session repeatability of ASL derived CBF values in each ROI for the single-PLD and multi-PLD protocols. First, we visualized scatter plots of the CBF values in WB, GM, WM and PVWM and quantitatively assessed the similarities of the values obtained in the two scans using Pearson's correlation coefficient. Thereafter, we used Bland Altman plots as another approach to visualize their intra-session repeatability. For each subject, method and ROI, we computed the within-subject coefficient of variation (wsCV) as the standard deviation of the two CBF values normalized by their mean. The summary wsCV measure for all the subjects were obtained as the root mean square of the individual wsCV values. Their 95% confidence intervals and statistical comparisons with other ROIs were obtained using bootstrapping methods. A p value of less than 0.05 was considered significant in any statistical analysis. We also aimed to compute the reproducibility of PVWM CBF using [^{15}O]-water PET, however the latter did not include arterial blood sampling needed for calculating absolute CBF. Hence, we computed relative PVWM CBF by dividing by the whole brain (WB) CBF, reported the corresponding wsCV for PET and compared that with single and multi PLD ASL.

2.4.2. Comparison of ASL CBF values with [^{15}O]-water PET measurements—For comparison across modalities, we considered the average ROI CBF of the two scans. Since [^{15}O]-water PET measurements did not provide absolute CBF measurements, the intermodal analysis focused on relative CBF in the GM, WM, and PVWM computed by dividing the respective ROI CBF by the WB CBF. We visualized the data using scatter plots and computed the Pearson's correlation coefficient to obtain a quantitative summary measure of similarity. In addition to comparing the ASL with PET measurements, we also compared the relative CBF measurements obtained with the single PLD and multi PLD ASL measurements.

2.4.3. Measurement of PVWM ATT—Finally, we measured the arterial transit time (ATT) of the PVWM region in individual subjects from the multi-PLD ASL data. For comparison we used the 10th and 90th percentile ATT values in both GM and WM. We

aimed to assess if ATT of the PVWM is of the same order as other regions of the brain, which would suggest that PVWM CBF can be measured with conventional ASL protocols.

3. Results

Multi PLD ASL data of one session of one subject was discarded from all analysis due to presence of visual artifacts. Table 1 shows summary statistics of the ASL derived ROI CBF values for each scan obtained with both single PLD and multi PLD acquisitions. The wsCV corresponding to their intra-session reliability and their 95% confidence intervals are also shown in the table.

Fig. 2 shows the intra-session repeatability of the ASL derived CBF values in each ROI. The top row shows scatter plots of the CBF values in the different ROIs and for each ASL protocol obtained from the two scans. Unity line references are shown in each plot and the Pearson's correlation coefficients are provided in each plot. The middle and bottom rows show Bland Altman plots for each ROI and ASL protocol. The PVWM ROIs have numerically larger variabilities, although of the same order, compared to the other ROIs. When the wsCV values corresponding to PVWM were compared statistically with the other ROIs, only that of WB was found to be significantly lower ($p = 0.046$ uncorrected for multiple comparisons) than PVWM in single PLD acquisition, and not for the other protocol-ROI combinations. The wsCV values in single and multi PLD ASL did not differ significantly. The wsCV of relative PVWM CBF (computed by normalizing by whole brain CBF) obtained with $[^{15}O]$-water PET was 5.1 (3.2,6.9)%, which was not statistically significantly different from that obtained with single PLD or multi PLD ASL whose wsCV values for relative PVWM CBF were 5.6 (3.5,7.4) and 5.0 (3.7,6.3) respectively.

Fig. 3 shows correlations between normalized ROI CBF values obtained with different methods. All the ROI CBF values between modalities were significantly correlated. The correlations with PVWM CBF were significantly lower than WM for single PLD versus PET ($p = 0.02$ uncorrected) and single PLD versus multi PLD ($p = 0.03$ uncorrected), but not for other ROI-protocol combinations. Surprisingly, the correlation with GM was significantly lower ($p = 0.04$ uncorrected) than WM for the single PLD acquisition. None of the differences in correlation coefficients was significant after correcting for multiple comparisons. In all the plots, the points are mostly scattered close to the unity line demonstrating similar GM-WM contrast after correcting for partial volume errors.

Fig. 4 shows the group averaged relative CBF maps obtained with each modality without correction for partial volume errors. CBF maps obtained with $[^{15}O]$-water PET are visibly sharper than those acquired with ASL. As can be seen in the images for all modalities, CBF values are lower in the periventricular region, and this reduction is distributed anisotropically around the caps of the lateral ventricles demonstrating that this distribution is not primarily driven by partial volume effects. The CBF gradient from deep WM to PVWM is however most prominent in PET data and least prominent in the single PLD ASL acquisition.

Fig. 5 shows the mean arterial transit times (ATT) in the PVWM ROI for all the subjects. The average ATT across subjects is 1.27 ± 0.27s. For comparison, the 10 and 90 percentile

ATT values in GM and WM are also shown. The plot suggests that ATT values for voxels in the PVWM region are not outliers within the cerebral arterial circulation.

4. Discussion

We evaluated CBF in the PVWM ROI using both single and multi PLD ASL acquisitions and demonstrated that it provided comparable test-retest reliability when compared to larger and more conventional ROIs. Furthermore, the correlations between ASL and [^{15}O]-water PET derived PVWM CBFs were comparable to the other ROIs, demonstrating that PVWM CBF can be reliably measured.

The within-session test-retest reliabilities were of the same order in all the ROIs, though the PVWM reliability in single PLD acquisition was lower than the WB ROI. Of note, the PVWM CBF is over an order of magnitude smaller than the other ROIs and are most weakly perfused resulting in lower signal to noise ratio than the other ROIs, so it was expected to show somewhat lower reliability than the other ROIs.

The CBF values from single-PLD and multi-PLD data were highly correlated and had comparable within session reliability. For a given scanning time, a single-PLD acquisition has advantage of providing higher SNR because of averaging with a greater number of label/control pairs, if acquired with optimal parameters. However, single-PLD data can still suffer from bias resulting from mismatch of the arterial transit time and choice of parameters, resulting in consistent error in both the sessions. In patients with cerebrovascular disease or in older subjects, the optimal PLD for a specific subject is not known in advance and hence multi-PLD acquisition can be more accurate (Fan et al., 2019; Wang et al., 2014).

Comparison of relative CBF obtained with [^{15}O]-water PET and ASL derived CBF values demonstrated significant correlations with values scattered close to the unity lines. Specifically, the correlations obtained with PVWM CBF were not markedly different from the other ROIs. The correlations with GM were unexpectedly somewhat lower than that with WM CBF. Although we corrected for partial volume errors, there can still be errors associated with the correction techniques that can potentially affect GM more than WM due to relatively thin cortical regions than WM volume. Future work using higher resolution ASL MRI would be expected to improve intermodality correlations in CBF. The CBF values obtained with single and multi PLD acquisitions were highly correlated, including those in the PVWM ROI. Hence the recommended single PLD ASL in Alsop et al. (2015), that does not account for ATT, can still be used to measure PVWM CBF, at least in healthy adults.

The ATT values of PVWM were relatively longer than the average ATT of GM and WM, but they are not so long that they cannot be measured with conventional ASL acquisition protocols. Note that the ATT reported here only represents the time for the labeled blood to reach the voxel of interest. The time to reach the microvasculature or tissue can be longer, but that should not affect CBF quantification at the voxel level.

In conclusion, we demonstrated that with current advanced ASL acquisition strategies, CBF in the weakly perfused PVWM can be measured with comparable reliability to other commonly evaluated ROIs. A limitation of this study is that PET acquisitions lacked arterial

sampling and so comparisons between ASL CBF and PET CBF used relative CBF values. Another limitation is the use of a middle-aged cohort. Older and diseased subjects with compromised cerebrovasculature might have lower reliability and longer arterial transit time in the PVWM ROI compared to that reported here, the reliability of PVWM CBF still needs to be confirmed in these populations.

Acknowledgements

References

Alsop DC, Detre JA, 1996. Reduced transit-time sensitivity in noninvasive magnetic resonance imaging of human cerebral blood flow. J. Cerebr. Blood Flow Metabol 16 (6), 1236–1249. 10.1097/00004647-199611000-00019.

Alsop DC, Detre JA, Golay X, Gunther M, Hendrikse J, Hernandez-Garcia L, Lu H, Macintosh BJ, Parkes LM, Smits M, van Osch MJ, Wang DJ, Wong EC, Zaharchuk G, 2015. Recommended implementation of arterial spin-labeled perfusion MRI for clinical applications: a consensus of the ISMRM perfusion study group and the European consortium for ASL in dementia. Magn. Reson. Med 73 (1), 102–116. 10.1002/mrm.25197. [PubMed: 24715426]

Asllani I, Borogovac A, Brown TR, 2008. Regression algorithm correcting for partial volume effects in arterial spin labeling MRI. Magn. Reson. Med 60 (6), 1362–1371. 10.1002/mrm.21670. [PubMed: 18828149]

Cannistraro RJ, Badi M, Eidelman BH, Dickson DW, Middlebrooks EH, Meschia JF, 2019. CNS small vessel disease: a clinical review. Neurology 92 (24), 1146–1156. 10.1212/WNL.0000000000007654. Lippincott Williams and Wilkins. [PubMed: 31142635]

Cuadrado-Godia E, Dwivedi P, Sharma S, Santiago AO, Gonzalez JR, Balcells M, Laird J, Turk M, Suri HS, Nicolaides A, Saba L, Khanna NN, Suri JS, 2018. Cerebral small vessel disease: a review focusing on pathophysiology, biomarkers, and machine learning strategies. J. Stroke 20 (3), 302–320. 10.5853/jos.2017.02922. Korean Stroke Society. [PubMed: 30309226]

Dai W, Robson PM, Shankaranarayanan A, Alsop DC, 2012. Reduced resolution transit delay prescan for quantitative continuous arterial spin labeling perfusion imaging. Magn. Reson. Med 67 (5), 1252–1265. 10.1002/mrm.23103. [PubMed: 22084006]

Detre JA, Alsop DC, Vives LR, Maccotta L, Teener JW, Raps EC, 1998. Noninvasive MRI evaluation of cerebral blood flow in cerebrovascular disease. Neurology 50 (3), 633–641. http://www.ncbi.nlm.nih.gov/pubmed/9521248. [PubMed: 9521248]

Detre JA, Leigh JS, Williams DS, Koretsky AP, 1992. Perfusion imaging. Magn. Reson. Med 23 (1), 37–45. http://www.ncbi.nlm.nih.gov/pubmed/1734182. [PubMed: 1734182]

Dolui S, Li Z, Nasrallah IM, Detre JA, Wolk DA, 2020. Arterial spin labeling versus 18F-FDG-PET to identify mild cognitive impairment. Neuroimage: Clin. 25 10.1016/j.nicl.2019.102146.

Dolui S, Tisdall D, Vidorreta M, Jacobs DR, Nasrallah IM, Bryan RN, Wolk DA, Detre JA, 2019. Characterizing a perfusion-based periventricular small vessel region of interest. Neuroimage: Clin. 23 10.1016/j.nicl.2019.101897.

Dolui S, Vidorreta M, Wang Z, Nasrallah IM, Alavi A, Wolk DA, Detre JA, 2017. Comparison of PASL, PCASL, and background-suppressed 3D PCASL in mild cognitive impairment. Hum. Brain Mapp 38 (10) 10.1002/hbm.23732.

Dolui S, Wang Z, Wang DJJ, Mattay R, Finkel M, Elliott M, Desiderio L, Inglis B, Mueller B, Stafford RB, Launer LJ, Jacobs DR, Bryan RN, Detre JA, 2016. Comparison of non-invasive MRI measurements of cerebral blood flow in a large multisite cohort. J. Cerebr. Blood Flow Metabol 36 (7) 10.1177/0271678X16646124.

Fan AP, Jahanian H, Holdsworth SJ, Zaharchuk G, 2016. Comparison of cerebral blood flow measurement with [15O]-water positron emission tomography and arterial spin labeling magnetic

resonance imaging: a systematic review. J. Cerebr. Blood Flow Metabol 36 (5), 842–861. 10.1177/0271678X16636393.

Fan Audrey P., Guo J, Khalighi MM, Gulaka PK, Shen B, Park JH, Gandhi H, Holley D, Rutledge O, Singh P, Haywood T, Steinberg GK, Chin FT, Zaharchuk G, 2017. Long-delay arterial spin labeling provides more accurate cerebral blood flow measurements in moyamoya patients: a simultaneous positron emission tomography/MRI study. Stroke 48 (9), 2441–2449. 10.1161/STROKEAHA.117.017773. [PubMed: 28765286]

Fan Audrey P., Khalighi MM, Guo J, Ishii Y, Rosenberg J, Wardak M, Park JH, Shen B, Holley D, Gandhi H, Haywood T, Singh P, Steinberg GK, Chin FT, Zaharchuk G, 2019. Identifying hypoperfusion in moyamoya disease with arterial spin labeling and an [15O]-Water positron emission tomography/magnetic resonance imaging normative database. Stroke 50 (2), 373–380. 10.1161/STROKEAHA.118.023426. [PubMed: 30636572]

Grant AM, Deller TW, Khalighi MM, Maramraju SH, Delso G, Levin CS, 2016. NEMA NU 2–2012 performance studies for the SiPM-based ToF-PET component of the GE SIGNA PET/MR system. Med. Phys 43 (5), 2334–2343. 10.1118/1.4945416. [PubMed: 27147345]

Gunther M, Bock M, Schad LR, 2001. Arterial spin labeling in combination with a look-locker sampling strategy: inflow turbo-sampling EPI-FAIR (ITS-FAIR). Magn. Reson. Med 46 (5), 974–984. 10.1002/mrm.1284. [PubMed: 11675650]

Habes M, Erus G, Toledo JB, Zhang T, Bryan N, Launer LJ, Rosseel Y, Janowitz D, Doshi J, Van der Auwera S, von Sarnowski B, Hegenscheid K, Hosten N, Homuth G, Volzke H, Schminke U, Hoffmann W, Grabe HJ, Davatzikos C, 2016. White matter hyperintensities and imaging patterns of brain ageing in the general population. Brain 139 (Pt 4), 1164–1179. 10.1093/brain/aww008. [PubMed: 26912649]

Holland CM, Smith EE, Csapo I, Gurol ME, Brylka DA, Killiany RJ, Blacker D, Albert MS, Guttmann CR, Greenberg SM, 2008. Spatial distribution of white-matter hyperintensities in Alzheimer disease, cerebral amyloid angiopathy, and healthy aging. Stroke 39 (4), 1127–1133. 10.1161/STROKEAHA.107.497438. [PubMed: 18292383]

Lee S, Viqar F, Zimmerman ME, Narkhede A, Tosto G, Benzinger TL, Marcus DS, Fagan AM, Goate A, Fox NC, Cairns NJ, Holtzman DM, Buckles V, Ghetti B, McDade E, Martins RN, Saykin AJ, Masters CL, Ringman JM, et al. , 2016. White matter hyperintensities are a core feature of Alzheimer's disease: evidence from the dominantly inherited Alzheimer network. Ann. Neurol 79 (6), 929–939. 10.1002/ana.24647. [PubMed: 27016429]

Moody DM, Bell MA, Challa VR, 1990. Features of the cerebral vascular pattern that predict vulnerability to perfusion or oxygenation deficiency: an anatomic study. Am. J. Neuroradiol 11 (3).

Nasrallah IM, Hsieh M-K, Erus G, Battapady H, Dolui S, Detre JA, Launer LJ, Jacobs DR, Davatzikos C, Bryan RN, 2019. White matter lesion penumbra shows abnormalities on structural and physiologic MRIs in the coronary artery risk development in young adults cohort. Am. J. Neuroradiol 40 (8) 10.3174/ajnr.A6119.

Pantoni L, 2010. Cerebral small vessel disease: from pathogenesis and clinical characteristics to therapeutic challenges. Lancet Neurol. 9 (7), 689–701. 10.1016/S1474-4422(10)70104-6. Lancet Neurol. [PubMed: 20610345]

Petr J, Mutsaerts H, De Vita E, Steketee RME, Smits M, Nederveen AJ, Hofheinz F, van den Hoff J, Asllani I, 2018. Effects of systematic partial volume errors on the estimation of gray matter cerebral blood flow with arterial spin labeling MRI. Magma 31 (6), 725–734. 10.1007/s10334-018-0691-y. [PubMed: 29916058]

Prins ND, van Dijk EJ, den Heijer T, Vermeer SE, Jolles J, Koudstaal PJ, Hofman A, Breteler MM, 2005. Cerebral small-vessel disease and decline in information processing speed, executive function and memory. Brain 128 (Pt 9), 2034–2041. 10.1093/brain/awh553. [PubMed: 15947059]

Promjunyakul N, Lahna D, Kaye JA, Dodge HH, Erten-Lyons D, Rooney WD, Silbert LC, 2015. Characterizing the white matter hyperintensity penumbra with cerebral blood flow measures. Neuroimage Clin 8, 224–229. 10.1016/j.nicl.2015.04.012. [PubMed: 26106546]

Promjunyakul NO, Dodge HH, Lahna D, Boespflug EL, Kaye JA, Rooney WD, Silbert LC, 2018. Baseline NAWM structural integrity and CBF predict periventricular WMH expansion over time. Neurology 90 (24), e2119–e2126. 10.1212/WNL.0000000000005684. [PubMed: 29769375]

Shi Y, Thrippleton MJ, Makin SD, Marshall I, Geerlings MI, de Craen AJ, van Buchem MA, Wardlaw JM, 2016. Cerebral blood flow in small vessel disease: a systematic review and meta-analysis. J. Cerebr. Blood Flow Metabol 36 (10), 1653–1667. 10.1177/0271678X16662891.

van Gelderen P, de Zwart JA, Duyn JH, 2008. Pittfalls of MRI measurement of white matter perfusion based on arterial spin labeling. Magn. Reson. Med 59 (4), 788–795. 10.1002/mrm.21515. [PubMed: 18383289]

Wang DJ, Alger JR, Qiao JX, Gunther M, Pope WB, Saver JL, Salamon N, Liebeskind DS, Investigators US, 2013. Multi-delay multi-parametric arterial spin-labeled perfusion MRI in acute ischemic stroke - comparison with dynamic susceptibility contrast enhanced perfusion imaging. Neuroimage Clin 3, 1–7. 10.1016/j.nicl.2013.06.017. [PubMed: 24159561]

Wang R, Yu S, Alger JR, Zuo Z, Chen J, Wang R, An J, Wang B, Zhao J, Xue R, Wang DJ, 2014. Multi-delay arterial spin labeling perfusion MRI in moyamoya disease–comparison with CT perfusion imaging. Eur. Radiol 24 (5), 1135–1144. 10.1007/s00330-014-3098-9. [PubMed: 24557051]

Wardlaw JM, Smith EE, Biessels GJ, Cordonnier C, Fazekas F, Frayne R, Lindley RI, O'Brien JT, Barkhof F, Benavente OR, Black SE, Brayne C, Breteler M, Chabriat H, Decarli C, de Leeuw FE, Doubal F, Duering M, Fox NC, et al. , 2013. Neuroimaging standards for research into small vessel disease and its contribution to ageing and neurodegeneration. Lancet Neurol. 12 (8), 822–838. 10.1016/S1474-4422(13)70124-8. [PubMed: 23867200]

Werner P, Barthel H, Drzezga A, Sabri O, 2015. Current status and future role of brain PET/MRI in clinical and research settings. Eur. J. Nucl. Med. Mol. Imag 42 (3), 512–526. 10.1007/s00259-014-2970-9. Springer Berlin.

Xu G, Rowley HA, Wu G, Alsop DC, Shankaranarayanan A, Dowling M, Christian BT, Oakes TR, Johnson SC, 2010. Reliability and precision of pseudocontinuous arterial spin labeling perfusion MRI on 3.0 T and comparison with 15O-water PET in elderly subjects at risk for Alzheimer's disease. NMR Biomed. 23 (3), 286–293. 10.1002/nbm.1462. [PubMed: 19953503]

Zhang K, Herzog H, Mauler J, Filss C, Okell TW, Kops ER, Tellmann L, Fischer T, Brocke B, Sturm W, Coenen HH, Shah NJ, 2014. Comparison of cerebral blood flow acquired by simultaneous [15O]water positron emission tomography and arterial spin labeling magnetic resonance imaging. J. Cerebr. Blood Flow Metabol 34 (8), 1373–1380. 10.1038/jcbfm.2014.92.

Zhang X, Ronen I, Kan HE, Teeuwisse WM, van Osch MJ, 2016. Time-efficient measurement of multi-phase arterial spin labeling MR signal in white matter. NMR Biomed. 29 (11), 1519–1525. 10.1002/nbm.3603. [PubMed: 27594277]
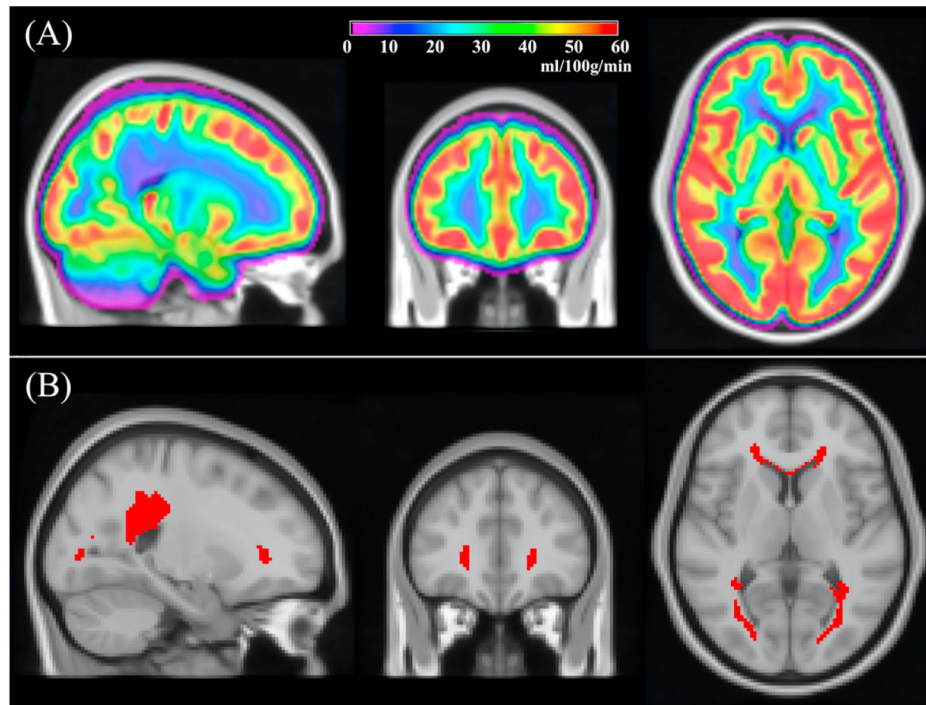
Fig. 1.
(A) Group averaged CBF obtained from 436 subjects (age = 50.4 ± 3.5 years, 54% female) from the NHLBI Coronary Artery Risk Development in Young Adults (CARDIA) study; (B) A periventricular white matter (PVWM) region of interest (ROI) obtained by thresholding the group averaged map in (A) to CBF<12.5 ml/100 g/min.
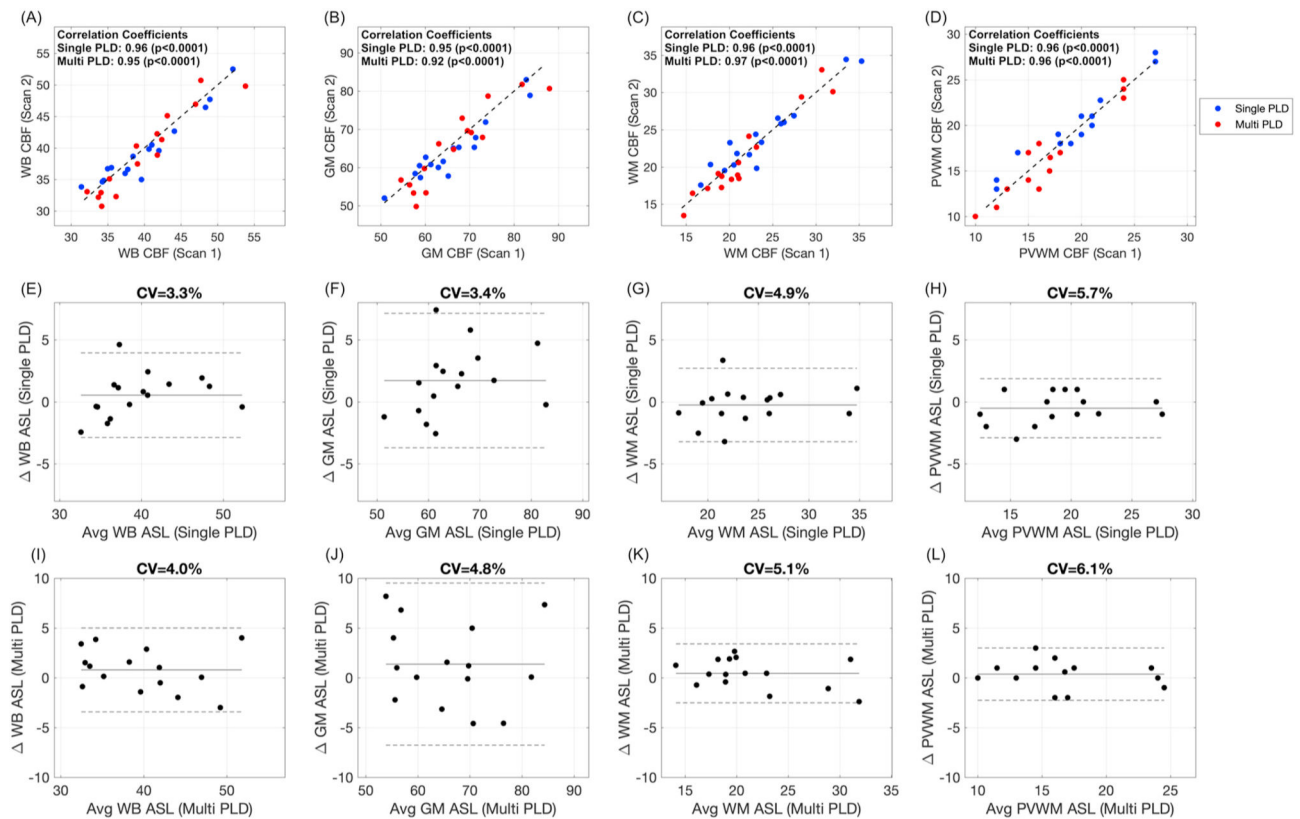
Fig. 2.
(A)–(D): Scatter plots comparing the (A) whole brain (WB) CBF, (B) gray matter (GM) CBF, (C) white matter (WM) CBF and (D) periventricular WM (PVWM) CBF obtained from the two sessions using single-PLD (shown in blue) and multi-PLD (shown in red) ASL. The black lines correspond to the unity line. (E)–(H) Bland Altman plots corresponding to (E) WB CBF, (F) GM CBF, (G) WM CBF and (H) PVWM CBF using the two sessions of single PLD data; (I)–(L) Bland Altman Plots corresponding to (I) WB CBF, (J) GM CBF, (K) WM CBF and (L) PVWM CBF using the two sessions of multi PLD data. CBF is expressed in ml/100 g/min. (For interpretation of the references to colour in this figure legend, the reader is referred to the Web version of this article.)
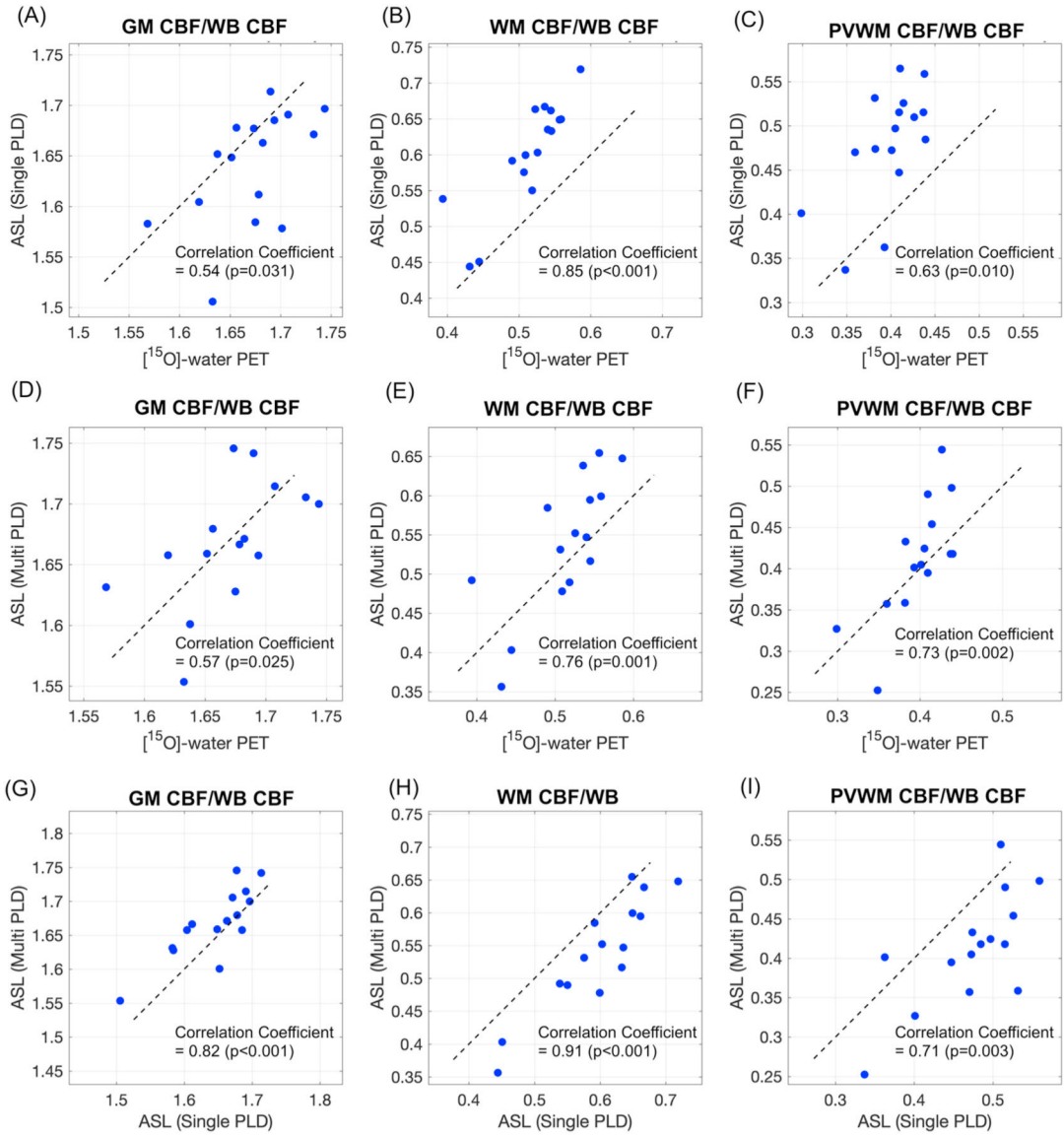
Fig. 3.
Scatter plots comparing the normalized CBF values (A)–(C) between [^{15}O]-water PET and Single PLD ASL in (A) Gray Matter (GM), (B) White Matter (WM) and (C) Periventricular White Matter (PVWM); (D)–(F) between [^{15}O]-water PET and Multi PLD ASL in (D) GM, (E) WM and (F) PVWM; and (G)–(I) between Single PLD and Multi PLD ASL in (G) GM, (H) WM and (I) PVWM. The normalizations in each case were obtained using whole brain (WB) CBF values. The dotted black lines in each plot correspond to the unity line.
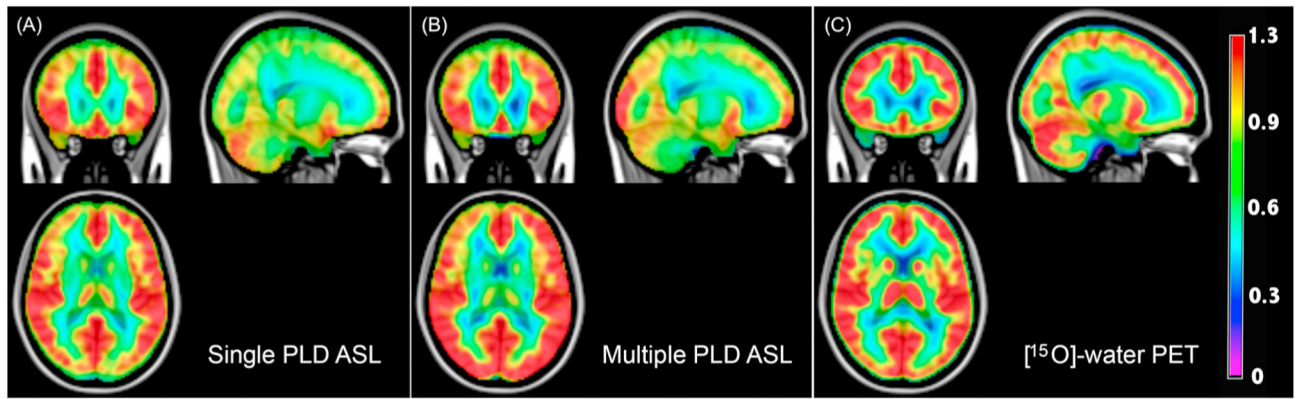
Fig. 4.
Group averaged relative CBF obtained with (A) single PLD ASL, (B) multi PLD ASL and (C) and [15O]-water PET. The relative CBF for each subject was obtained by normalizing by whole brain CBF values.
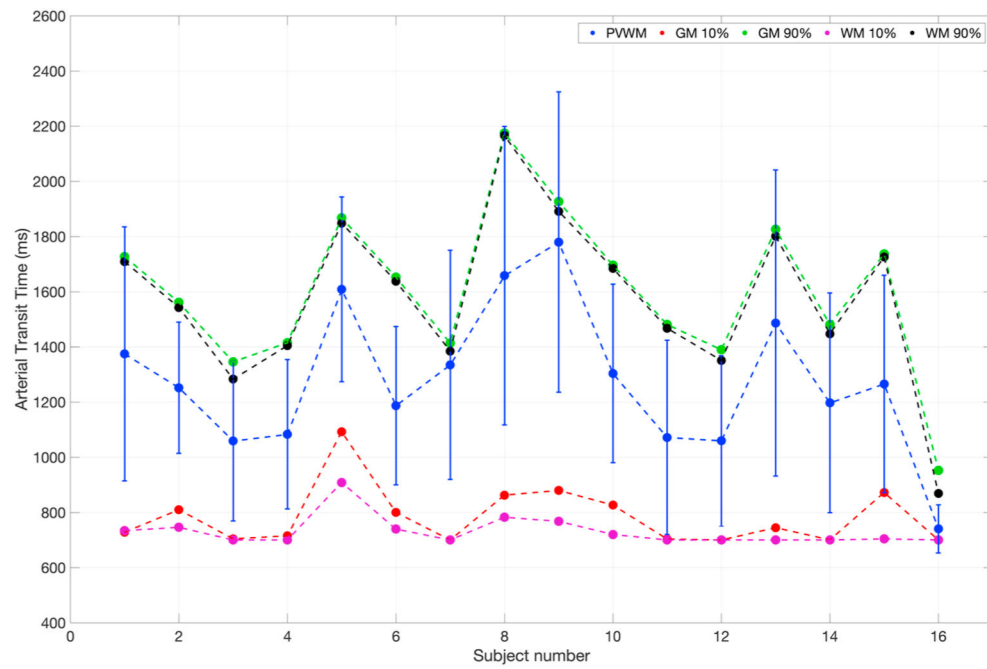
Fig. 5.
Arterial transit times (ATTs) of the periventricular white matter (PVWM) region of interest
(ROI) in each subject. The standard deviations within the ROI for each subject are shown
as error bars. For comparison, the 10th and 90th percentile arterial transit time values of the
gray and white matter ROIs are also shown.

Table 1

Descriptive Statistics of ASL derived CBF values.

	Single PLD ASL			Multi PLD ASL		
	Scan 1	Scan 2	wsCV (95% CI)	Scan 1	Scan 2	wsCV (95% CI)
WB CBF	40.1 ± 5.9	39.5 ± 5.4	3.3 (2.0,4.6)[a]	40.1 ± 6.2	39.3 ± 6.7	4.0 (2.7,5.2)
GM CBF	66.0 ± 8.9	64.3 ± 8.0	3.4 (2.2,4.7)	66.7 ± 9.7	65.4 ± 10.4	4.8 (2.0,6.4)
WM CBF	23.9 ± 5.1	24.1 ± 4.8	4.9 (2.4,6.7)	21.6 ± 5.1	21.2 ± 5.6	5.1 (3.7,6.3)
PVWM CBF	18.9 ± 4.5	19.4 ± 4.2	5.7 (3.4,7.7)	16.6 ± 4.4	16.2 ± 4.6	6.1 (3.8,8.3)

[a]Represents that the wsCV for the specific ROI – protocol combination was significantly lower than the wsCV of PVWM for that specific protocol (fourth row).